EVALUATION OF TI15MO ALLOY MANUFACTURED BY DMLS FROM ELEMENTAL POWDERS

T. Dzogbewu[1*]

[1*] Department of Mechanical and Mechatronic Engineering
Central University of Technology, Bloemfontein, South Africa
(Corresponding author: thydzo@yahoo.fr)

ABSTRACT

The paper presents a study of in-situ alloying Ti15wt%Mo powder mixture by Direct Metal Laser Sintering (DMLS) process. Titanium and molybdenum powders of similar particle size distributions were mixed, and the powder mixture was used to create DMLS samples using two different scanning strategies. Rescanning was also investigated as a means of ensuring homogeneity of the microstructure. The DMLS built materials were evaluated in terms of optical microscopy, SEM, Vickers microhardness and tensile testing. It was found that, in all cases, partially melted Mo particles remained in the microstructure. This causes variance in hardness and tensile properties, as can be expected from an inhomogeneous microstructure.

1. INTRODUCTION

Ti6Al4V has being used extensively for biomedical applications due to its outstanding biological response. However, it is well documented in the literature that its Elastic modulus (80-120 GPa) is far above that of human bone tissues (10-30 GPa) [1] which has limit its use as a structural biomedical material. For replacing a critical damage load bearing structure such as the femur, the implant must have a good combination of low Elastic modulus and high ductility [2-4]. These limitations of Ti6Al4V has triggered a search for a more preferable biomaterial.
ß-type titanium alloys have been the focus of interest probably due to the fact that bone tissues respond better in ß-type Ti alloys than in (α+ß)-type Ti alloys [4-5]. A host of researchers have used the conventional methods to produce ß-type Ti alloys such as Ti15Mo and reported that the mechanical properties of the Ti15Mo are more suitable for structural biomedical applications than Ti6Al4V [3-7]; due to its high ductility, good mechanical properties, excellent corrosion resistance, and well characterized biological response. Very recently a profound revelation was made by Disegi *et al*. [4] of the Ti15Mo alloy and the results were incorporated into ASTM F 2066 implant material standard.

Xie *et al*. [8] produced Ti-xMo (x=4, 6, 8 and 10 wt. %) alloys using the selective laser sintering method. It was found that the mechanical properties of the Ti-xMo porous structures do not only depends on the pore properties but also on the microstructure. Collins *et al*. [9] carried out detailed studies of microhardness and microstructural evolution of Ti-xMo alloys by laser engineered net-shaping (LENS) process. It was concluded that the alloy is very sensitive to the Mo compositions. Recently Vrancken *et al*. [10] conducted in-situ alloying with mixture of Ti6Al4V and Mo (10 wt.%) powders and focused on the solidification mechanism, microstructure, mechanical properties and response to heat treatment of the novel alloy and compared the results to Ti6Al4V. Elastic modulus of 73 GPa and remarkable elongation to 20% was reported as compared to 7.3% for Ti6Al4V alloy.

It is therefore of prime importance to further unearth its promising biomechanical properties with relatively newer technology (DMLS) to harness the full potential of the alloy for biomedical application. The importance of producing structural bearing ß-titanium alloys by DMLS, the increasing research interest in the subject matter and the huge unexploited potential of ß-titanium alloys is the driving force behind the current research.

2. METHODOLOGY AND RESULTS

2.1 METHODOLOGY

The experiments were conducted with pure Ti (Cp Ti, grade 2) and Mo powders procured from TLS Technik. The powders were spherical argon-atomized powders. The Ti powder has the following chemical composition in wt.%: Ti (bal.), O (0.17), Fe (0.062), C (0.006), H (0.002), N (0.012). The 10th, 50th and 90th percentiles of equivalent diameter (weighted by volume) of the powder Ti particles were d10=11.6 µm, d50=24.6 µm and d90=38.4 µm, for Mo powder they were d10=10.9 µm, d50=22.4 µm and d90=31.9 µm. 85 wt.% of the Cp Ti powder was mechanically mixed with 15 wt.% of the Mo. The mixture was dried in an oven for about 15 hours at the temperature of 85°C. The powder mixture was stirred for 30 minutes to ensure the heating is evenly done to enhance free flowing of the powder.

EOS M 280 DMLS machine was used for in situ alloying the elemental powders (Ti15Mo). A preliminary analysis was conducted to determine the optimum process parameters for the selected alloy (85wt% of pure Ti + 15wt% of Mo) by forming and studying single tracks and single layers according to well-known procedures described in the literature [11-13] and published [14]. The optimum process parameters in the previous studies (laser power of 150 W and 350 W with corresponding scanning speeds of 1.0 m/s and 2.4 m/s respectively) were used to produce as-built samples for microstructural and mechanical properties investigation.

Cubes of dimension 10 mm $\times$ 10 mm $\times$ 7 mm (length $\times$ width $\times$ thickness) were produced for microstructure and microhardness analysis. For the microstructural studies, the samples were removed from the build plate via wire Electrical Discharge Machining and section/cross-section into smaller unit for mounting. Struers CitoPress- 1 machine was used for mounting the samples in MultiFast non-conductive resin. The mounted samples were grinded and polished with Struers Tegramin-25 according to the protocol suggested by Struers for Ti-based alloys and subsequently etched with Kroll's reagent. The microstructural examinations were conducted by an optical microscope (OM). The distribution of Mo in Cp Ti was done with Scanning Electron Microscope (SEM). Microhardness of the samples was measured at 200 g loading with FM-700 Digital Vickers Microhardness Tester in polished cross-sections cut perpendicular to the building direction (40 measurements for each cross-section).

Mini-tensile test samples were produced from the Ti15Mo powder mixture with the EOS M 280 machine. The samples were rectangular in shape with 10 mm gauge length, 2 mm width and 1 mm thickness [15]. The samples were prepared according to E8/E8M ASTM standard. The tensile tests were carried out using MTS Criterion Model 43 Electromechanical Universal Test System machine at room temperature with a strain rate of

0.5 mm/min. The surface roughness of the mini samples was measured with Surftest SJ-210 portable surface roughness tester from Mitutoyo Corporation.

2.2 RESULTS AND DISCUSSIONS

2.2.1 Microstructure

Due to the layerwise (step-by-step) building process used by the DMLS technology the microstructure of a DMLS build parts are different when viewed from different planes (Figure 1). A commonly used coordinate system is the scanning plane x-y and the built direction z. During the DMLS process, the individual scan tracks propagate in the scanning direction [12, 16] due to the directional heat flux and the large thermal gradient [17]. The directional variation in the microstructure of DMLS built parts is due to the very high rate of heating and cooling (10^{-4}–10^{-6} K/s) [18, 19] simultaneously cum the solidification mechanisms [17]. It is also worth mentioning that other scholars are of the view that the rate of heating and cooling during DMLS is still a matter of research [20].

The microstructures obtained in the current experiment generally consists of three distinct phases. With optical microscope photos it can be seen partially melted Mo particles, the gray and dark varying-contrast areas (Figure 1a-b). From the SEM analysis, the gray and dark varying contract sections represent the dissolved Mo in the Ti alloy matrix (Figures 1c-d). The white contrasting areas at BSE mode by SEM were found as partially melted Mo particles. The concentration of Mo in grey areas (similar to the point A in Fig. 1d) was 7.5-16 wt%. Bright grey areas had higher concentration of Mo, it was 24.7wt% in the point B in Figure 1d, for example. In whole, observed average concentrations of Mo in the alloy correspond well to the bi-modal α+β microstructures.

The constituted microstructure demonstrates overlapping of subsequent scan tracks as a result of the optimum hatch distance and the selected scanning strategy employed. The overlapping edges are of curve shape (approximately parabolic – red curves, Figure 1b) from the side view which signify the welding of each layer onto the layers that surround it.

Dark field micrograph reveals the presence of needles (fine acicular martensite) inside the prior ß grains of Ti alloy (Figure 2a-b) due to the high cooling rates during the DMLS process [21-22]. Regions of beta cubic phase also were formed as cellular dendritic structure during solidification (Figure 2c). Cellular dendritic structures were associated with Mo particles; it was confirmed by higher concentration of Mo in these regions [14].

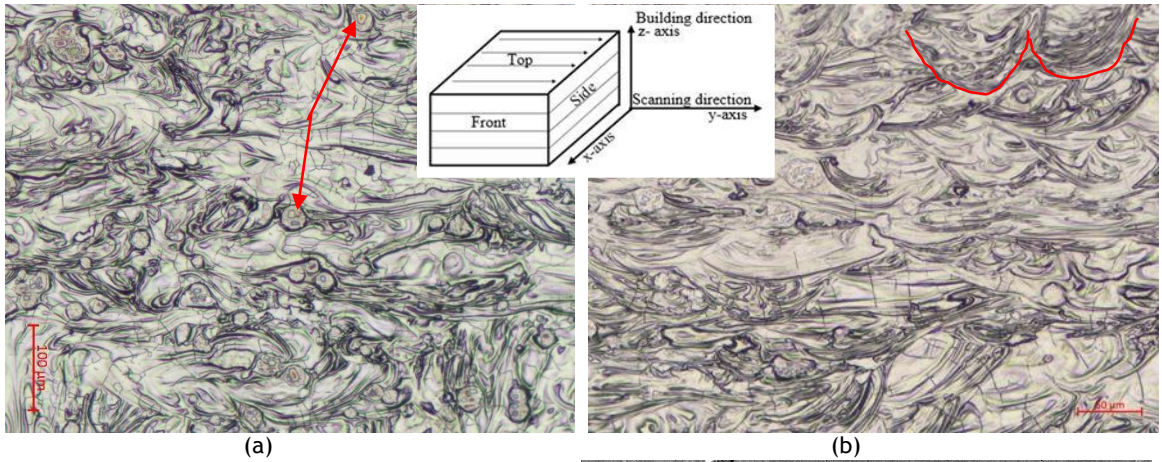

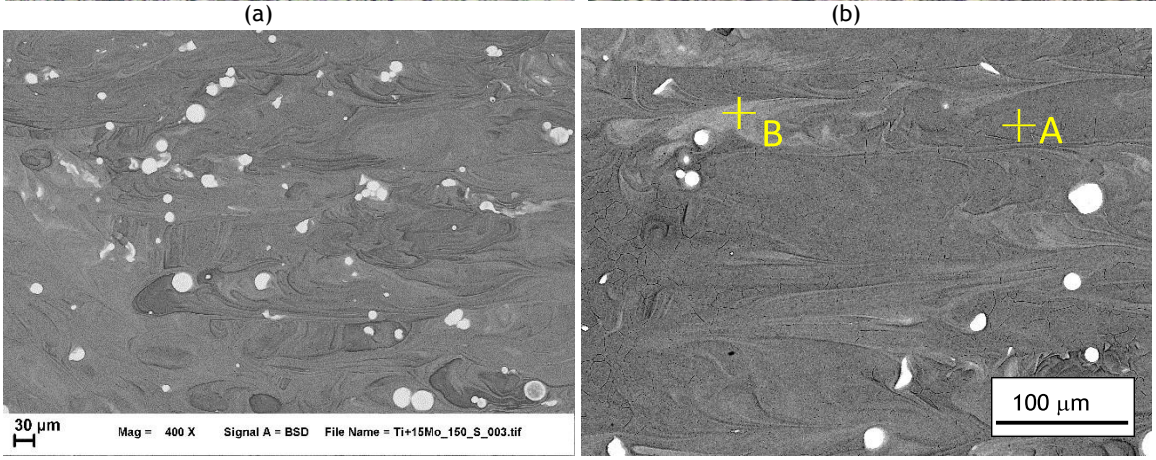

(c) (d)

Figure 1: Ti15Mo microstructure produce at laser power of 150 W at speed of 1.0 m/s: (a) top view (unmelted Mo particles – red arrows) (b) side view (parabolic shape – red curves) SEM image in BSE mode of top cross-section (c, d)

Generally, from all the views (Figure 1-2) there were partially melted Mo particles distributed randomly in the alloy matrix. The distribution and mixing of the particles in the solidified melt pool could be related to convective flow in the liquid melt pool [23]. The Mo was not able to melt completely due to the thermo- physical difference between the two materials. Mo has a melting point of 2623°C [24] while Ti has a melting point in the range of 1650-1670°C [25]. Secondly, the laser reflectance of Mo is higher than that of Ti [26]. Ti would absorb more laser radiation than Mo. These thermophysical differences induce the partial melting of the Mo leading to the formation of Mo particle - Ti alloy matrix microstructure.

A rescanning strategy was employed, whereby after each layer is built before a new powder deposition the previously solidified layer was rescanned. This strategy was expected to melt any unmelted Mo particle before a new powder deposition; as presented in the earlier publication [14]. The rescanning strategy did not have any significant effect on the unmelted Mo particles (Figure 3).

The microstructure of samples produces at 350 W with a corresponding scanning speed of 2.4 m/s (Figure 4) were similar to those of 150 W at a scanning speed of 1.0 m/s. However, there seem to be more unmelted Mo particle at laser power of 350 W than 150 W. This is due to the fact that at a high scanning speed, the dwelling time of the laser at a particular spot on the powder bed reduces [27]. The relative high laser scanning speed of 2.4 m/s at 350 W implies that not sufficient time to melt the Mo particles before the propagation of the laser beam to the next spot. As a result of the short stay at a specific point, fewer Mo particles were melted at the laser power of 350 W with the relatively high scanning speed of 2.4 m/s as compared to laser power of 150 W with the slower scanning speed of 1.0 m/s. Becker *et al*. [28] noted that the high scan speed minimises heat transfer.

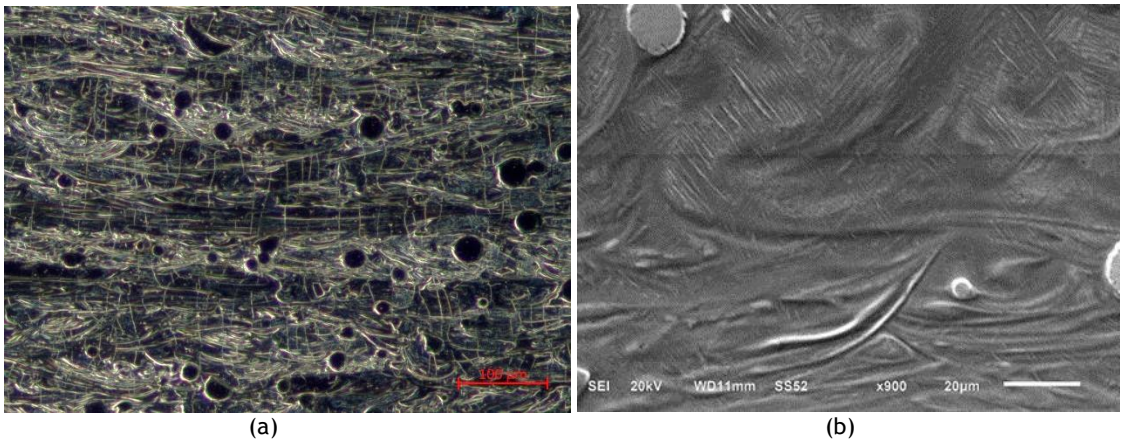

(a) (b)

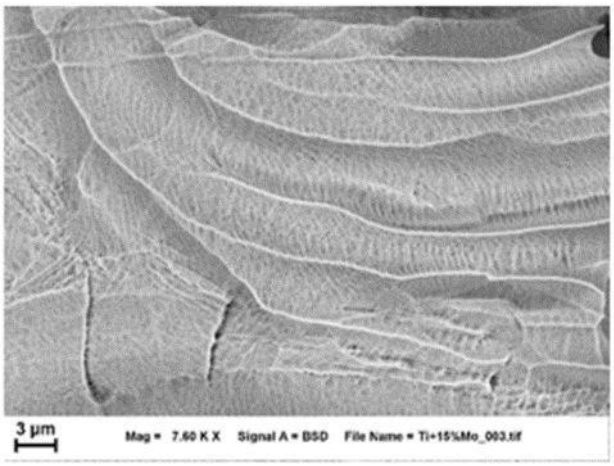

(c)

Figure 2: Microstructure in dark field by optical microscope at laser power of 150W (a) SEM micrograph showing needles at laser power of 150 W (b) SEM micrograph showing cellular dendrite at laser power of 150 W (c)

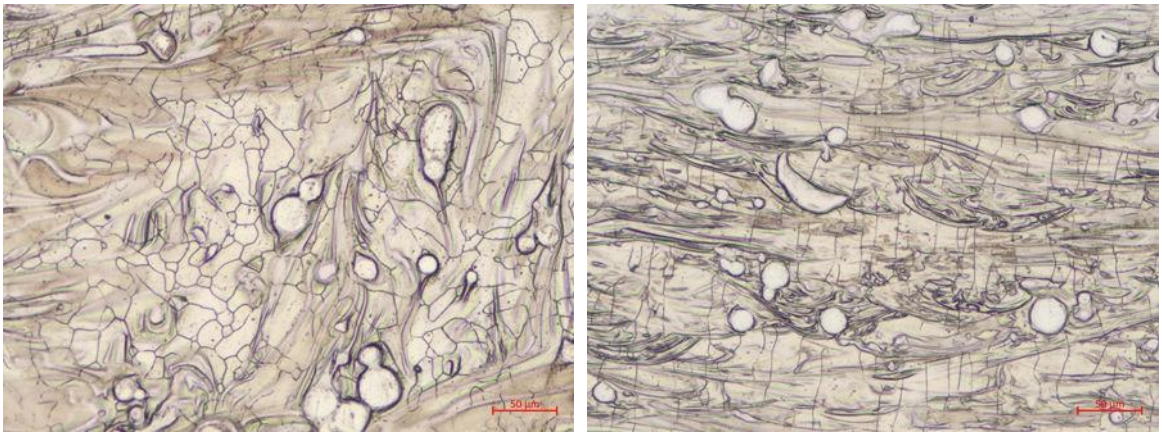

(a) (b)

Figure 3: Microstructure of Ti15Mo samples rescan at a laser power of 150 W at speed of 1.0 m/s: (a) top view (b) representing both side and front views.

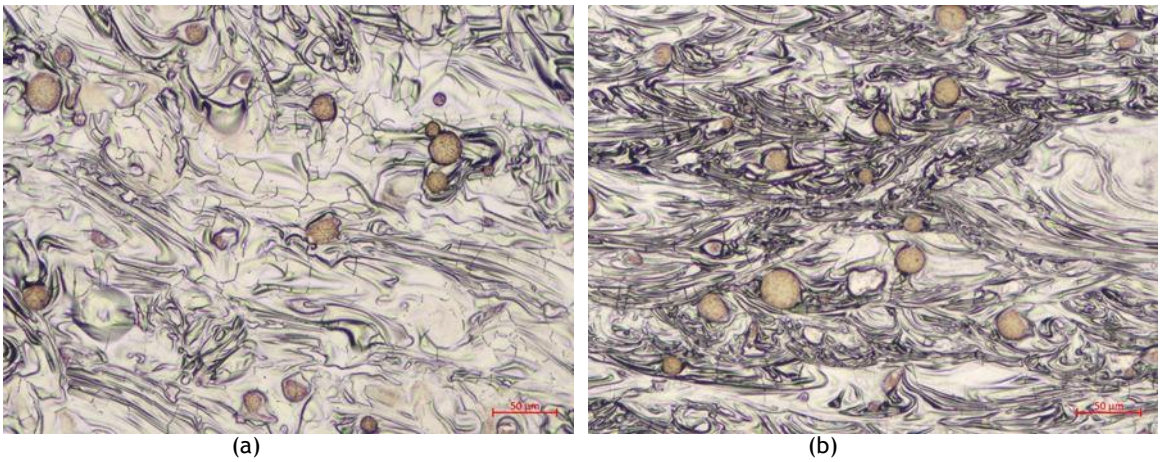

(a) (b)

Figure 4: Microstructure of Ti15Mo samples scan at laser power of 350 W at speed of 2.4 m/s: (a) top view (b) representing side and front views.

From the current results it could be speculated that reducing the laser scanning speed could trigger complete melting of the Mo particles. But as pointed out by Yadroitsev *et al*. [16] the DMLS process parameters are not linearly related, rather only a careful combination of the laser power and scanning speed that could yield optimum results.

2.2.2 Porosity

For all the different sets of samples at the two process parameters (laser power of 150 W and 350 W at scanning speeds of 1.0 m/s and 2.4 m/s respectively), there were found some pores in-between the solidified layers (x-y plane) (Figure 5). The location of the pores justified the assumption that the pores occur due to in- homogenous powder delivery. During DMLS process when the surface of the previously solidified layer is uneven with deep valleys and peaks the next powder distribution would be uneven. The uneven powder deposition would lead to pore formation in-between the solidified layers known as interlayer porosity [29-31]. The uneven powder deposition is currently assumed to occur due to the agglomeration of the mixed powder. The experimental powders were mixed mechanically which might have provoked the agglomeration of the powder during the DMLS process. The interlayer pores are a detrimental feature in DMLS built parts as far as the mechanical properties and fatigue life of biomedical objects are concerned since it compromises structural integrity and contributes strongly to premature and unexpected structural failure of the parts [31].

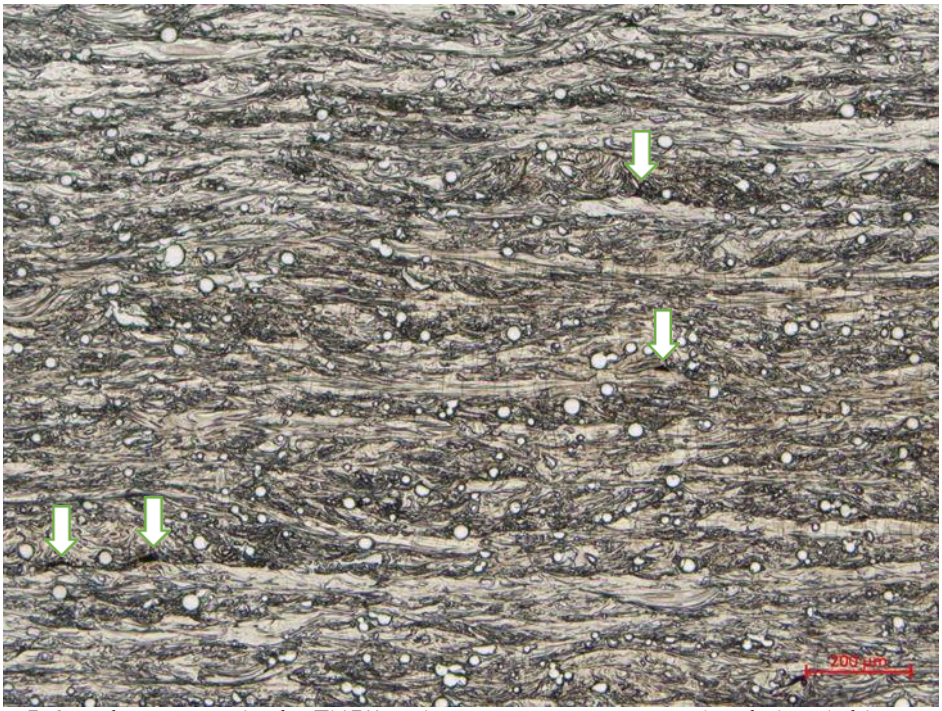

Figure 5: Interlayer pores in the Ti15Mo microstructure – cross sectional view (white arrows).

The interlayer pores were slightly bigger for the rescan samples at both process parameters. As mentioned earlier laser absorption increase with increasing surface roughness [32-33]. The irregular solidified layers after the single scan would certainly increase the laser energy absorption during the rescanning process which would lead to a higher temperature and more prominent flow of the molten pool. The high speed lateral liquid metal during the rescanning process is more susceptible of trapping gas bubbles [22] and therefore forming bigger interlayer pores at the bottom of the track. Yadroitsev, *et al*. [12] also noted that since rescanning process does not involve new powder deposition, the interaction of the laser beams with the solid material (thermal conductivity, heat transfer, laser absorptivity and reflectivity) is completely different. These thermophysical differences can lead to higher energy input during the rescanning process. "Higher energy input can cause high temperatures, overheating, boiling and evaporation of material in the laser interaction zone and irregular track formation" which could be the reason for the slightly bigger interlayer pores for the rescanned samples.

2.2.3 Mechanical Properties Investigations

2.2.3.1 Microhardness Test

The microhardness of the front and side views of the as built Ti15Mo samples were investigated in order to study the anisotropic behavior typically of DMLS build parts [21,22, 34, 35]. The Vickers's hardness numbers (VHN) presented in Table 2.1 attest to the fact that DMLS build parts are not holistically homogenous throughout the bulk material. This is generally link to the layer-wise building process and the direction of heat conduction. However, for the current experiment, the random distribution of partially melted Mo particles also contributed significantly to the varied microhardness values in the Ti15Mo material matrix.

Table 2.1 Microhardness values of the Ti15Mo alloy at the optimum process parameters

Process parameters	Samples	Front (HV)	Side (HV)
150 W, 1.0 m/s	Single scan	426 ±27	441±40
	Rescan	439±32	443±45
350 W, 2.4 m/s	Singe scan	436±24	436±28
	Rescan	443±19	441±26

It could be observed that the microhardness values varied which could be attributed to the random distribution of the Mo particles in the Ti15Mo material. Nonetheless, taking the mean of the scan and rescan results the microhardness of the two process parameters are almost the same; 438 ± 36 for 150 W at a scanning speed of 1.0 m/s and 439 ± 24 for the 350 W at a scanning speed of 2.4 m/s. These values correlate with the result of Collins *et al*. [9]. They produced a compositionally graded structure of Ti-xMo (x= 0-25at.%) by laser engineered net-shaping (LENS™) and reported the highest microhardness value of 450 HVN at 10wt.% Mo concentration and noted that the microhardness value of the samples reduces with increasing Mo content. Therefore, obtaining microhardness value of ~ 440 HV indicate a reduction in VHN with increase in Mo centration. The microhardness value recorded for the unmelted Mo particles randomly dispersed in the Ti15Mo alloy at the two optimum process parameters were almost the same (Figure 6).

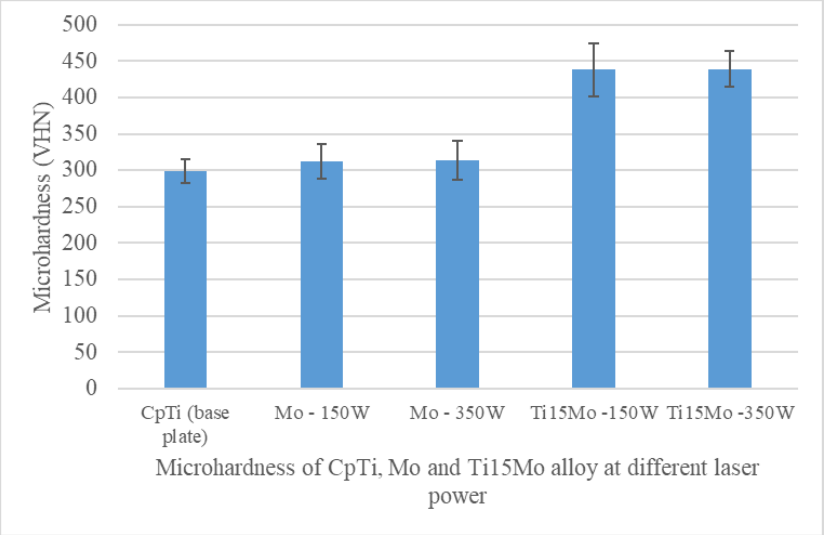

Figure 6: Microhardness of the base Cp Ti plate, and DMLS Mo and Ti15Mo alloy

2.2.3.2 Fracture analysis

The fracture surface and geometry of the fracture of a metal is dependent on the microstructure of the metal [36]. Generally, after a metal undergoes a tensile test the fracture surface is rough and irregular as in the case of Ti15Mo samples (Figure 6a). SEM analysis reveals the occurrence of complex ductile/brittle fracture (Figure 6b) with brittle fracture predominance. The interior of Figure 6a reveals the predominance of brittle fracture. At a higher magnification (Figure 6b) there was evidence of areas of ductile tearing (quasi-cleavage fracture). This type of fracture is due to the occurrence of both ductile (dimples) and brittle fracture together on a single fracture surface (mixed mode). van Zyl et al. (2016) examined the fracture surface of Ti6Al4V mini sample produced by DMLS and observed ductile-brittle fracture with ductile predominance contrary to the brittle predominance observed for the Ti15Mo samples.

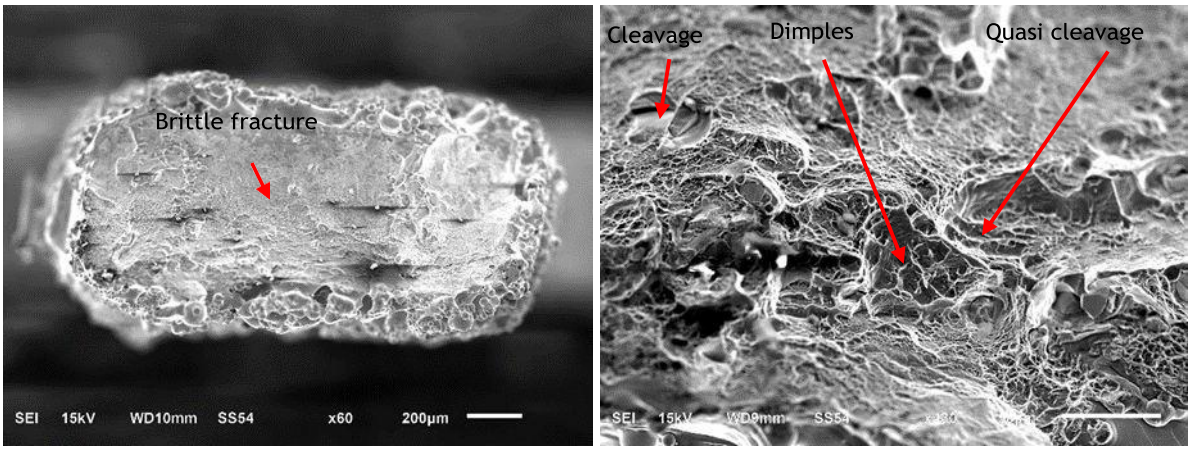

(a) (b)

Figure 6: SEM micrograph of fracture surface – total view (a) and fracture surface at higher magnification showing predominant ductile fracture with some cleavage features at fracture surface (b).

2.2.3.3 Tensile test

Based on the above-detailed analysis samples were produced at a laser power of 150 W at a scanning speed of 1.0 m/s for tensile test analysis. As generally demonstrated and accepted in literature, the stress is determined as the ratio between the applied load and the nominal cross-section of the samples while the strain is taking as the ratio between the normal height and the increased height after the tensile test.

Five mini samples were pulled for the tensile test investigation. The average ultimate tensile strength value obtained for the five Ti15Mo mini sample was lower than that of Ti6Al4V mini sample reported by van Zyl et al. [15]. The average elongation at break for the five Ti15Mo samples was also lower than that of Ti6Al4V alloy mini sample (Table 2.2). Though the DMLS process has a great freedom of design which makes it a prime choice for biomedical applications the fast rate of heating and cooling which lead to martensitic formation

reduces the ductility of the material greatly, as in DMLS Ti6Al4V alloy. In present experiments, partially melted Mo particles were randomly distributed in Ti alloy. Inhomogeneity in sintered material and residual stress can decrease ductility.

Table 2.2 Comparison of the average tensile properties values of Ti15Mo and Ti6Al4V Mini samples

Sample	UTS (MPa)	Elongation (%)	Microhardness (HV)	Roughness		Ref.
				Ra	Rz	
Ti15Mo	894±24	2.8±1.7	441±2	21.27±0.6	123.50±3.94	
Ti6Al4V	1243±49	6.6±0.4	389±14.8	21.7±4.37	125.2±20.49	[15]

3. CONCLUSION

The DMLS process successfully demonstrated its potency of sintering elemental powders (*in-situ* alloying). As demonstrated using DMLS to process powder mixtures of different materials would certainly broaden the material database of additive manufacturing. It would also permit the material scientist to mix different elemental powders for specific applications.

In DMLS pure Ti and Mo powders mixture with similar particle size distribution, resulted DMLS material had low level of porosity, but was nonhomogeneous. Other approach, with smaller Mo particles has to be introduced for full melting at higher fusion temperature Mo component.

Also inherent high rate of heating and cooling simultaneously introduce significant amount of martensitic phase into the mini-sample which lead to substantial reduction in the ductility of the samples.

The ultimate aim of producing biomedical objects of high ductility for structural bearing implants in a single step by the DMLS process could not be achieved. However, post processing strategies such as heat treatment could still be employed to achieve this aim. Producing implants with high ductility would greatly reduce implants failures associated with stress shielding effect which would translate to improve life for implant patients.

ACKNOWLEDGEMENTS

This work is based on research supported by the South African Research Chairs Initiative of the Department of Science and Technology and the National Research Foundation of South Africa (Grant №97994) and the Collaborative Programme in Additive Manufacturing (Contract №CSIR-NLC-CPAM-15-MOA-CUT-01).

REFERENCES

[1] **Niinomi, M., Narushima, T., & Nakai, M.** 2015. *Advances in Metallic Biomatrial. Tissues, Matrials and Biological Reactions*, Vol.3, Heidelberg, DE: Springer.

[2] **Ho, W.F., Ju, C.P. & Lin, J.C.** 1999. Structure and properties of cast binary Ti–Mo alloys, *Biomaterials*, 20(22), pp. 2115-2122.

[3] **Disegi, J.** 2003. *Wrought Titanium-15% Molybdenum Implant Material*, Original Instruments and Implants of the Association for the Study of International Fixation—AO ASIF.

[4] **Disegi, J., Roach, M., McMillan, R. & Shultzabarger, B.** 2016. Alpha plus beta annealed and aged Ti-15 Mo alloy for high strength implant applications, *Journal of Biomedical Materials Research Part B: Applied Biomaterials*.

[5] **Niinomi, M., Kuroda, D., Fukunaga, K.I., Morinaga, M., Kato, Y., Yashiro, T. & Suzuki, A.** 1999. Corrosion wear fracture of new β type biomedical titanium alloys, *Materials Science and Engineering: A*, 263(2), pp. 193-199.

[6] **Oliveira, N., Aleixo, G., Caram R. & Guastaldi, A.** 2007. Development of Ti–Mo alloys for biomedical applications: microstructure and electrochemical characterization, *Materials Science and Engineering: A*, 452, pp. 727-731.

[7] **Júnior, M., Severino, J., Nogueira, R., Araújo, R., Donato, T., Arana-Chavez, V., Claro, A., Moraes, J., Buzalaf M. & Grandini, C.** 2011. Preparation and characterization of Ti-15Mo alloy used as biomaterial, *Materials Research*, 14(1) pp. 107-112.

[8] **Xie, F., He, X., Lv, Y., Wu, M., He, X. & Qu, X.** 2015. Selective laser sintered porous Ti–(4–10) Mo alloys for biomedical applications: Structural characteristics, Mechanical properties and corrosion behaviour, *Corrosion Science*, 95, pp. 117-124.

[9] **Collins, P., Banerjee, R., Banerjee, S. & Fraser, H.** 2003. Laser deposition of compositionally graded titanium–vanadium and titanium–molybdenum alloys, *Materials Science and Engineering: A*, 352(1), pp. 118-128.

[10] **Vrancken, B., Thijs, L., Kruth, J. & Van Humbeeck, J.** 2014. Microstructure and mechanical properties of a novel β titanium metallic composite by selective laser melting, *Acta Materialia*, 68, pp. 150-158.

[11] **Yadroitsev, I., Yadroitsava, I., Bertrand, P. & Smurov, I.** 2012. Factor analysis of selective laser melting process parameters and geometrical characteristics of synthesized single tracks, *Rapid Prototyping Journal*, 3(18), pp. 201-208.

[12] **Yadroitsev, I., Krakhmalev, P. & Yadroitsava, I.** 2015. Hierarchical design principles of selective laser melting for high quality metallic objects, *Additive Manufacturing*, 7, pp. 45-56.

[13] **Yadroitsava, I, Els, J, Booysen, G. & Yadroitsev, I.** 2015. Peculiarities of single track formation from TI6AL4V alloy at different laser power densities by selective laser melting, *South African Journal of Industrial Engineering,* 26(3), pp. 86-95.

[14] **Dzogbewu, T.C, Yadroitsev, I, Krakhmalev, P, Yadroitsava, I & Du Plessis, A**. 2017. Optimal process parameters for in-situ alloyed Ti15Mo structures by Direct Metal Laser Sintering, *Proceedings of the 28th Annual International Solid Freeform Fabrication Symposium*, Austin Texas, August 7-9, 2017. (In press)

[15] **van Zyl, I., Moletsane, M., Krakhmalev, P., Yadroitsava, I. & Yadroitsev, I.** 2016. Validation of miniaturised tensile testing on DMLS TI6AL4V (ELI) specimens, *South African Journal of Industrial Engineering*, 27(3), pp. 192-200.

[16] **Yadroitsev, I., Gusarov, A., Yadroitsava, I. & Smurov, I.** 2010. Single track formation in selective laser melting of metal powders, *Journal of Materials Processing Technology*, 210(12), pp. 1624-1631.

[17] **Kruth, J.P., Badrossamay, M., Yasa, E., Deckers, J., Thijs, L. & Van Humbeeck, J.** 2010. Part and material properties in selective laser melting of metals, *In Proceedings of the 16th international symposium on electromachining*.

[18] **Roberts, I.A., Wang, C.J., Esterlein, R., Stanford, M. & Mynors, D.J.** 2009. A three-dimensional finite element analysis of the temperature field during laser melting of metal powders in additive layer manufacturing, *International Journal of Machine Tools and Manufacture*, 49(12), pp. 916-923.

[19] **Brandl, E. & Greitemeier, D**. 2012. Microstructure of additive layer manufactured Ti–6Al–4V after exceptional post heat treatments, *Materials Letters*, 81, pp. 84-87.

[20] **Yan, M. & Yu, P.** 2015. An Overview of Densification, Microstructure and Mechanical Property of Additively Manufactured Ti-6Al-4V—Comparison among Selective Laser Melting, Electron Beam Melting, Laser Metal Deposition and Selective Laser Sintering, and with Conventional Powder, *In Sintering Techniques of Materials,* InTech.

[21] **Thijs, L., Verhaeghe, F., Craeghs, T., Van Humbeeck, J. & Kruth, J.P.** 2010. A study of the microstructural evolution during selective laser melting of Ti–6Al–4V, *Acta Materialia*, 58(9), pp. 3303-3312.

[22] **Simonelli, M., Tse, Y.Y. & Tuck, C.** 2012. Microstructure of Ti-6Al-4V produced by selective laser melting, *In Journal of Physics,* 371(1) pp. 012084.

[23] **Khairallah, S.A., Anderson, A.T., Rubenchik, A. & King, W.E.** 2016. Laser powder-bed fusion additive manufacturing: Physics of complex melt flow and formation mechanisms of pores, spatter, and denudation zones, *Acta Materialia*, 108, pp. 36-45.

[24] **AZO**, 2015. AZO materials. [Online] Available at: http://www.azom.com [Accessed 10 May 2017].

[25] **ASM**, 2016. ASM aerospace specification metals Inc. [Online Available at: http://www.matweb.com/ [Accessed 10 May 2017].

[26] **Lynch, D., Hunter, W. & Palik, E.** 1985. *Handbook of optical constants of solids*, Orlando: Academic press.

[27] **Manakari, V., Parande, G. & Gupta, M.** 2016. Selective Laser Melting of Magnesium and Magnesium Alloy Powders: A Review, *Metals*, 7(1), pp. 2.

[28] **Becker, T., Van Rooyen, M. & Dimitrov, D**. 2015. Heat treatment of Ti-6Al-4V produced by lasercusing, *South African Journal of Industrial Engineering*, 26(2), pp. 93-103.

[29] **Hofmeister, W. & Griffith, M.** 2001. Solidification in direct metal deposition by LENS processing, *Journal of the Minerals, Metals and Materials Society*, 53(9), pp. 30-34.

[30] **Su, W.N., Erasenthiran, P. & Dickens, P.M.** 2003. Investigation of fully dense laser sintering of tool steel powder using a pulsed Nd: YAG (neodymium-doped yttrium aluminium garnet) laser, *Proceedings of the Institution of Mechanical Engineers, Part C: Journal of Mechanical Engineering Science*, 217(1), pp. 127-138.

[31] **Ahsan, M.N., Bradley, R. & Pinkerton, A.J.** 2011. Microcomputed tomography analysis of intralayer porosity generation in laser direct metal deposition and its causes, *Journal of laser applications*, 23(2), pp. 022009.

[32] **Gharbi, M., Peyre, P., Gorny, C., Carin, M., Morville, S., Le Masson, P., Carron, D. & Fabbro, R.** 2013. Influence of various process conditions on surface finishes induced by the direct metal deposition laser technique on a Ti-6Al-4V alloy, *Journal of materials processing technology*, 213(5), pp. 791-800.

[33] **Wang, Y.** 2008. Mechanical properties and microstructure of laser sintered and starch consolidated iron-based powders, Doctoral dissertation, Karlstads universitet.

[34] **Vrancken, B., Thijs, L., Kruth, J.P. & Van Humbeeck, J.** 2012. Heat treatment of Ti6Al4V produced by Selective Laser Melting: Microstructure and mechanical properties, *Journal of Alloys and Compounds*, 541, pp. 177-185.

[35] **Vrancken, B., Cain, V., Knutsen, R. & Van Humbeeck, J.** 2014. Residual stress via the contour method in compact tension specimens produced via selective laser melting, *Scripta Materialia*, 87, pp. 29-32.

[36] **Mandelbrot, B.B., Passoja, D.E. & Paullay, A.J.** 1984. Fractal character of fracture surfaces of metals, *Nature*, 308(5961), pp. 721-722.